Powder Technology, 72 (1992) 241–253

Aerated bunker discharge of fine dilating powders

C. E. D. Ouwerkerk*, H. J. Molenaar
Koninklijke/Shell-Laboratorium, Amsterdam (Shell Research B. V.), P.O. Box 3003, 1003 AA Amsterdam (Netherlands)
and M. J. W. Frank
Department of Chemical Engineering, University of Twente, P.O. Box 217, 7500 AE Enschede (Netherlands)

(Received October 30, 1991; in revised form April 6, 1992)

Abstract

The discharge rate of coarse powders (mean particle size >500 μm) from bunkers without aeration can be described by both empirical relations and theoretical models. In the case of small particles the discharge rate is largely overestimated. As the powder dilates during flow a negative pressure gradient develops near the hopper outlet, inducing an air flow into the hopper. This extra drag force decreases the discharge rate for fine particles. Aeration of the hopper through a porous cone section will create an opposite pressure gradient, and thereby increase the discharge rate. The aim of this investigation was to incorporate the dilation in an *ad hoc* way into the model of Altiner in order to improve its predictive power. To test the modified model we carried out experiments with a fluid catalytic cracking powder to study its discharge as a function of aeration. As the improved model needs a dilation parameter as input, the local bulk density was measured during flow at the outlet and at the bin/hopper junction using gamma-ray absorption. At the bin/hopper junction the bulk density was found to be independent of the discharge rate and equal to the bulk density at minimum fluidisation. At the outlet the bulk density goes through a maximum when the amount of aeration gas is increased. Without aeration gas a large dilation, *i.e.* a 15–35% lower bulk density, was observed. With these data the model predictions improved from 600% overestimation error to 25–90% underestimation for pure gravity discharge, and from 100% to 0–20% error for aerated discharge. However, the bulk density at the outlet cannot be predicted from the powder compressibility, as it seems to depend on dilation at fluidisation.

Introduction

Control of solids flow is essential in many types of process equipment. Usually this control is effected by means of mechanical valves with the disadvantages that they are subject to wear and that they only function well in a limited range of process conditions. Pneumatic flow control, if possible, is then to be preferred. The gravity discharge of powders from silos has been widely investigated, because it is a fairly simple and general operation, and because a vast amount of literature is available on stress and velocity distributions in silos.

In general, gravity discharge of coarse powders (mean particle diameter $d_p>500$ μm) from bunkers can be well predicted with empirical relations [1]. In the case of finer powders these relations overestimate the discharge rates by a wide margin (100–600%), due to the underpressure which develops near the vicinity of the orifice. This causes an air flow into the bunker, resulting in an extra drag force on the particles [2–4]. Aeration of the bunker near the orifice will give an opposite fluid pressure gradient and will therefore increase the mass flow.

In the more fundamental continuum mechanics approach, powder flow from hoppers is usually described by friction theories using Mohr–Coulomb plasticity laws [1]. In the modelling of flow patterns or stress profiles the material is then often assumed to be incompressible [1, 5, 6]. However, even for coarse particles ($d_p>500$ μm) measurement of the density near the outlet during discharge shows significant density gradients with up to 30% dilation [3, 7, 8]. To incorporate this effect, which reduces the discharge rate for smaller particles, into a model several investigators have assumed a dependence of density on the local mean stress level [2, 3, 9]. However, powder compressibilities are measured at much higher pressures (1–100 bar) than those present in bunkers, and result in much lower dilations than those experimentally observed near outlets, where solids stresses are almost zero [2–4].

With fine powders the interstitial air gradient causes an appreciable external pressure gradient under dilation,

*Present address: Shell Nederland Raffinaderij B. V., Vondelingenweg 601, 3196 KK Rotterdam/Pernis, Netherlands.

0032-5910/92/$5.00

complicating the problem to that of a real two-phase system. This is also the case when aeration gas is added to enhance the flow, both with coarse and with fine particles. For fine particles some authors start their description from flow from fluidised beds, using an inviscid flow theory [10], assuming that at the outlet the interparticle friction can be neglected due to the lubrication of the interstitial air flow. However, in this approach the prediction of the dilation and its link to other powder properties has not received much attention up to now. For our problem of the prediction of the aerated discharge of an A-powder the question was whether the large zero-stress dilation at the outlet could be explained by the amount of stable expansion at fluidisation.

For the aerated discharge of powders a relatively simple continuum model based on the assumption of an incompressible Mohr–Coulomb material has been described by Altiner [11, 12]. His experimental results show that it predicts both gravity and aerated discharge fairly well for large particles ($d_p > 200\ \mu m$) only, because the dilation at the outlet was not taken into account. For our purpose, a dilation was introduced in an *ad hoc* way into the theoretical model of Altiner.

This investigation comprises an experimental and a theoretical part. The experimental part includes the characterisation of the Fluid Catalytic Cracking (FCC) powder, needed as input for the computer model, and the measurement of the discharge rates of the powder from a bunker with a conical hopper. The discharge rate was measured using different amounts of aeration gas, while the amount of dilation was determined *in situ* using a gamma-ray absorption technique. The theoretical part includes the improvement of Altiner's model and the comparison of its predictions with the experimental results. At the same time an attempt is made to relate the measured amount of dilation to the fluidisation properties of the powder.

Theory

Introduction

First, the most well-known empirical relations will be presented for both gravity and aerated discharge. Next, a description of Altiner's model, together with our own extensions will be given.

Using dimensional analysis Beverloo proposed the following empirical correlation for solids discharge from circular apertures [1]:

$$W = 0.58\rho_b g^{0.5}(D_o - kd_p)^{2.5} \quad (1)$$

with k being a constant (about 1.4 for spheres) and ρ_b the bulk density of the material in its flowing state. kd_p refers to the 'vena contracta' – an annulus round the edge of the outlet, where no discharge can take place – to account for the increasing porosity near a wall. In incompressible flow the driving force is the specific weight $\rho_b g$, but when a powder dilates a second body force appears, namely a pressure difference across the orifice Δp_o. Then, the negative gauge pressure in the vicinity of the orifice decreases the mass flow rate, and injection of air near the orifice, *i.e.* applying a positive pressure difference across the outlet, increases the mass flow rate. Resnick *et al.* [13] modelled the pressurized flow of coarse solids from vessels using an energy balance over the orifice, resulting in W being proportional to $(g + \text{constant} \times \Delta p_o)^{0.5}$, with the constant depending on particle properties only. However, it is desirable to be able to predict this pressure difference from theory [2, 3]. Therefore, to give a description of the transition from packed-bed flow to suspension flow when aerating the material, it is necessary to take a more fundamental approach. Then, the flow properties of the powder in question and the permeability of the bed have to be taken into account.

Altiner's model

The assumptions in Altiner's model [11, 12] are the following:

- axi-symmetric hopper with radial (incompressible) flow of a cohesionless, free-flowing powder at a constant voidage
- an air flow Q_T is introduced over the lower part of the cone and is assumed to spread uniformly over the hopper angle
- no negative gauge pressure is created during the downflow, due to the assumption of incompressibility.

A small volume element of the material is shown in Fig. 1. The equation of motion for smooth walls ($\tau_{r\psi} = \tau_{\theta\psi} = \tau_{r\theta} = 0$) is as follows:

$$\rho_b v\ dv/dr + 1/r^2 d/dr(r^2\sigma_r) - (\sigma_\theta + \sigma_\psi)/r + dp/dr + \rho_b g \cos\theta = 0 \quad (2)$$

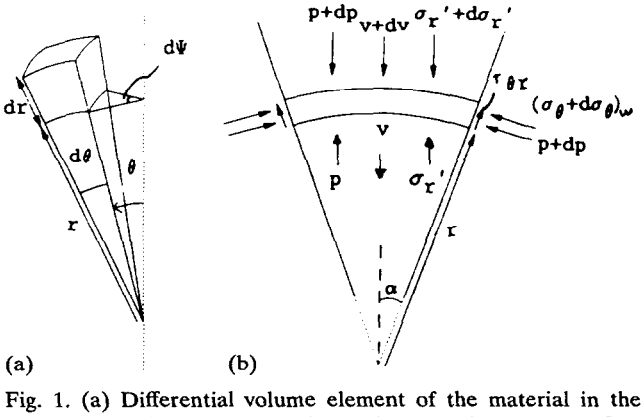

Fig. 1. (a) Differential volume element of the material in the hopper and (b) slice element in the hopper with the main flow and stress variables.

In steeply converging channels the material is in mass flow with passive solids stresses in the cone, *i.e.* $\sigma_\theta = K\sigma_r$. For frictionless walls $K = (1+\sin\delta)/(1-\sin\delta)$. For rough walls the constant K is replaced by $D_a F + ED_a/\tan\alpha$, with

$$D_a = (\sigma_r)_w/\overline{\sigma_r}$$
$$E = (\tau_{\theta r})_w/(\sigma_r)_w \qquad (3)$$
$$F = (\sigma_\theta)_w/(\sigma_r)_w$$

D_a, E and F can be calculated numerically from the assumptions of a radial stress field only, for example by using Jenike's Runge–Kutta numerical solution [14], or analytically using Walker's assumption of $\tau \div \theta$ [5]. With the Haar and Von Karman hypothesis that $\sigma_\psi = \sigma_\theta$, $\cos\theta \approx 1$ (small hopper angles) and $v = V/r^2$, with V defined as $W/2\pi\rho_b\,(1-\cos\alpha)$, it can be derived that

$$d\overline{\sigma_r}/dr + 2(1-K)\overline{\sigma_r}/r = 2\rho_b V^2/r^5 - dp/dr - \rho_b g \qquad (4)$$

To be able to solve the differential equation above, we need the fluid pressure gradient in the axi-symmetric hopper.

The following two additions to Altiner's model were made:
- on top of the hopper a bin is present
- the aeration section is not limited to the lower part of the cone, but can be varied in position (see Fig. 2).

The gas is brought into the hopper through a porous cone section (see Fig. 2). Altiner only used the lower part of the cone ($r_3 = r_0$), but as we want to vary the place of the aeration section in the experiments, a variable boundary r_3 is introduced. This introduces an extra section I. Further an extra section IV is introduced, to take the influence of a bin section into account.

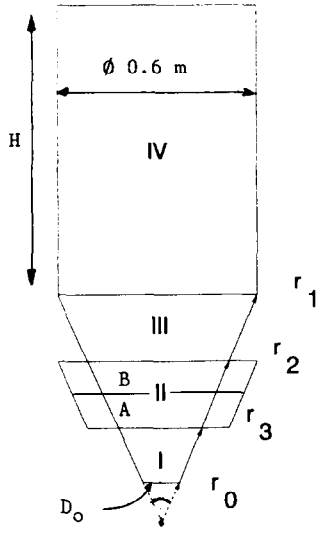

Fig. 2. Schematic drawing of the cylindrical bunker. In the experimental setup the aeration section II is divided into two parts A and B.

Assuming that the gas velocity is distributed uniformly over the whole conical aeration area the superficial inlet gas velocity is

$$U_\alpha = Q_T/\pi \sin\alpha(r_2^2 - r_3^2) \qquad (5)$$

Further a radius r_i is defined ($r_3 \leqslant r_i \leqslant r_2$) such that any gas entering above r_i flows towards the top of the particle bed and any gas entering below r_i goes through the orifice. As the flow rate in the distribution section changes with r, different equations are needed for the relative gas velocity u in the four sections of Fig. 2. With Darcy's equation

$$dp/dr = u/K_p \text{ with } K_p = d_p^2\epsilon^2/180(1-\epsilon)^2\mu \qquad (6)$$

and the four equations for u we have:

section I: $$dp/dr = A_a(r_i^2 - r_3^2)/r^2 \qquad (7)$$

section II: $$dp/dr = A_a(r_i^2 - r^2)/r^2 \qquad (8)$$

section III: $$dp/dr = -A_a(r_2^2 - r_i^2)/r^2 \qquad (9)$$

section IV: $$dp/dr = -A_a(r_2^2 - r_i^2)/r_1^2 \qquad (10)$$

with

$$A_a = U_\alpha \sin\alpha/2K_p\epsilon(1-\cos\alpha) \qquad (11)$$

By integrating these four differential equations with the boundary conditions $p = 0$ at $r = r_1 + H$ and $p = 0$ at $r = r_0$ and the condition that the pressure profile is continuous at the section boundaries, the value of r_i can be determined:

$$r_i^2 = (r_1^2 r_3^2 - 2r_0 r_1^2 r_3 + Hr_0 r_2^2 - r_0 r_1 r_2^2 + 2r_0 r_1^2 r_2)/(r_1^2 + Hr_0 - r_0 r_1) \qquad (12)$$

Then, the pressure distribution $p(r)$ follows from integration of eqns. (7) to (10)

section I: $$p = A_a(r_i^2 - r_3^2)(1/r_0 - 1/r) \qquad (13)$$

section II: $$p = A_a(r_i^2 - r_3^2)(1/r_0 - 1/r_3) + A_a r_i^2(1/r_3 - 1/r) - A_a r + A_a r_3 \qquad (14)$$

section III: $$p = A_a H(r_2^2 - r_i^2)/r_1^2 + A_a(r_2^2 - r_i^2)(1/r - 1/r_1) \qquad (15)$$

section IV: $$p = (H + r_1 - r)A_a H(r_2^2 - r_i^2)/r_1^2 \qquad (16)$$

with r_i as given in eqn. (12).

With the above pressure distributions, eqn. (4) can now be written as

$$d\sigma_r/dr + D\sigma_r/r = A/r^5 + B_i/r^2 + C_i \qquad (17)$$

where B_i and C_i are constants and are specific for the sections I, II and III. Integration of eqn. (17) leads to

$$r^D\sigma_r = r^{D-4}A/(D-4) + r^{D-1}B_i/(D-1) + r^{D+1}C_i/(D+1) + \text{constant} \quad (18)$$

The boundary conditions are $\sigma_r = 0$ at $r = r_0$ and $\sigma_r = \sigma_{r_1}$ at $r = r_1$. σ_{r_1} is calculated using Walters' stress model for axi-symmetric mass flow bunkers [6], which calculates stress profiles in bins and hoppers using a differential slice method. With the condition that the stress profile is continuous at the section boundaries, a value of the constant A can be determined and after introducing the dimensionless parameters.

$$z_2 = r_2/r_0, \quad z_3 = r_3/r_0, \quad z_m = r_m/r_0,$$
$$x = r/r_0 \text{ and } y = r_1/r_0 \quad (19)$$

one obtains

$$\begin{aligned} A(1-y^{D-4})/D-4) &= r_0^3(B_2 z_2^{D-1} + B_1 z_3^{D-1} - B_1 - B_2 z_3^{D-1} \\ &- B_3 z_2^{D-1} + B_3 y^{D-1})/(D-1) \\ &+ r_0^5(C_2 z_2^{D+1} + C_1 z_3^{D+1} - C_1 - C_2 z_3^{D+1} - C_3 z_2^{D+1} \\ &+ C_3 y^{D+1})/(D+1) - y^D r_0^4 \sigma_{r_1} \end{aligned} \quad (20)$$

From this equation, together with $W = V 2\pi\rho(1-\cos\alpha)$ and $2\rho V^2 = A$ (see eqns. (4) and (17)), the particle discharge rate W can be calculated.

The radial stress profile as a function of r can then be calculated as follows:

section I:
$$\begin{aligned} x^D r_0^4 \sigma_r &= A(x^{D-4} - 1)/(D-4) \\ &+ B_1 r_0^3 (x^{D-1} - 1)/(D-1) \\ &= + C_1 r_0^5 (x^{D+1} - 1)/(D+1) \end{aligned} \quad (21)$$

section II:
$$\begin{aligned} x^D r_0^4 \sigma_r &= A(x^{D-4} - 1)/(D-4) \\ &+ r_0^3(B_2 x^{D-1} + B_1 z_3^{D-1} \\ &- B_1 - B_2 z_3^{D-1})/(D-1) \\ &+ r_0^5(C_2 x^{D+1} + C_1 z_3^{D+1} \\ &- C_1 - C_2 z_3^{D+1})/(D+1) \end{aligned} \quad (22)$$

section III:
$$\begin{aligned} x^D r_0^4 \sigma_r &= A(x^{D-4} - y^{D-4})/(D-4) \\ &+ B_3 r_0^3 (x^{D-1} - y^{D-1})/ \\ &(D-1) + C_3 r_0^5 (x^{D+1} \\ &- y^{D+1})/(D+1) + y^D r_0^4 \sigma_{r_1} \end{aligned} \quad (23)$$

with A as defined by eqn. (17).

When gas is injected, the stress profile develops a minimum. As an example, the stress profiles for the 50 mm orifice are given in Fig. 3 for different values of Q_T. For a certain flow rate the stress minimum becomes zero. Calculating the location of this minimum by calculating $d\sigma_r/dr$ in section II would lead to a complicated equation, therefore Altiner uses the following estimation: $r_m \approx 0.5(r_i + r_2)$ [11, 12]. As a cohesionless material cannot support any tensile stresses, it is assumed that beyond this amount of gas no more reduction in stresses can occur. Therefore, this is the limiting air input for that system. An expression for the limiting air input is obtained by putting $\sigma_r = 0$ at $r = r_m$ in the stress eqn. (17). This gives an $A_{a,\,max}$ (cf. eqn. (11)), which is present in the constants B_i, C_i and A (see eqn. (17)):

$$\begin{aligned} A_{a,\,max}[G_1/r_0(D-1) + G_2 r_0/(D+1)] \\ = -qy^D\sigma_{r_1} - G_3 r_0/(D+1) \end{aligned} \quad (24)$$

with

$$q = (1 - z_m^{D-4})/(1 - y^{D-4}) \quad (25)$$

$$\begin{aligned} G_1 = &-r_i^2 z_m^{D-1} + r_3^2 z_3^{D-1} + r_i^2 - r_3^2 + q r_2^2 z_2^{D-1} - q r_3^2 z_3^{D-1} \\ &- q(r_i^2 - r_3^2) - q(r_2^2 - r_i^2) y^{D-1} \end{aligned} \quad (26)$$

$$G_2 = z_m^{D+1} - z_3^{D+1} - q z_2^{D+1} + q z_3^{D+1} \quad (27)$$

and

$$G_3 = q_b g(-z_m^{D+1} + 1 - q + q y^{D+1}) \quad (28)$$

From eqns. (5) and (11) it follows that

$$Q_{T,\,max} = A_{a,\,max} 2\pi K_p \epsilon (1 - \cos\alpha)(r_2^2 - r_3^2) \quad (29)$$

Introduction of the dilation

For small particles the powder expansion and the resulting negative pressure gradient, which develop at the outlet in case of zero aeration, have to be taken into account in the model. The fact that the flow ceases to be radial at the outlet, with the velocity proportional to $1/r^2$, disables Altiner's analytical solution, which would have led to solving another balance equation for the gas phase. To circumvent this we tested a simple *ad hoc* solution, assuming the dilation to be small and therefore the particle flow to be still almost radial. The same differential equation is solved, but the gas flow rate Q_T will be replaced by an effective flow rate

$$Q = Q_T - \delta Q \quad (30)$$

The second term is the amount of gas that has to flow into the hopper to compensate for the dilation $\delta\epsilon$. From Fig. 4 it follows that

$$\begin{aligned} \delta Q &= V_{out} - V_{in} = W/\rho_{b,\,out} - W/\rho_{b,\,in} \\ &= (\epsilon_{out} - \epsilon_{in}) W/[\rho_p(1-\epsilon_{in})(1-\epsilon_{out})] \end{aligned} \quad (31)$$

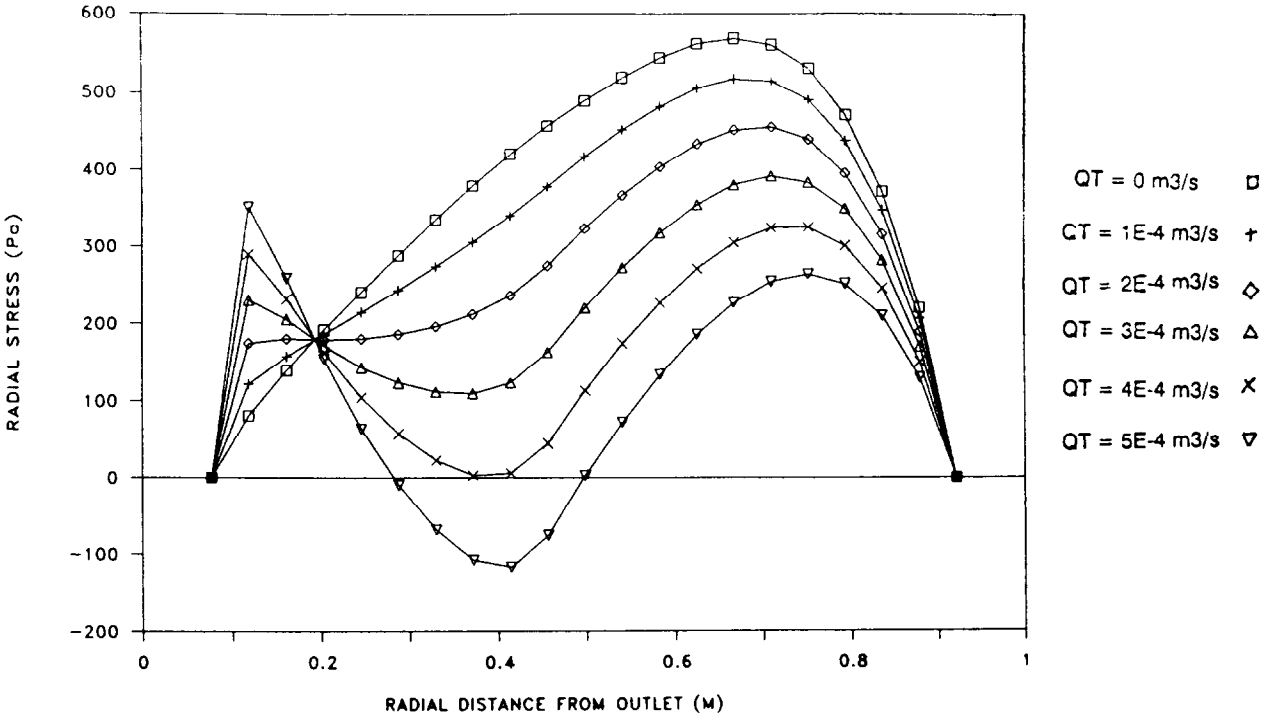

Fig. 3. Example radial solids stress profiles diameter as a function of aeration rate Q_T for the 50 mm outlet.

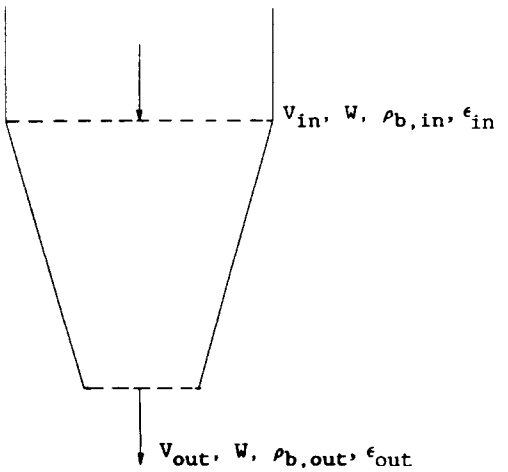

Fig. 4. Schematic drawing of the material dilation in the hopper.

and this leads, with $\rho_{b,\,in}=\rho_b$, to

$$\delta Q=\delta\epsilon W/[\rho_b(1-\epsilon_{in}-\delta\epsilon)] \tag{32}$$

A computer program was written to calculate for a given set of powder properties (including its dilation!) and bunker geometry the particle discharge rate W as well as the profiles along the hopper of the average radial stress σ_r, the fluid pressure p and the fluid pressure gradient dp/dr, all as a function of aeration rate Q_T.

Aerated discharge experiments

The bunker used in the experiments has a bin consisting of two aluminium cylinders each with a diameter of 0.6 m and a height of 1 m each. The conical hopper, with a half opening angle α of 19°, consists of four parts, two of which can be used to add the aeration gas (see Fig. 2). The hopper can be opened and closed with a slide valve. The discharge rate is determined from the weight-versus-time curve of a collecting vessel below. During most experiments the bed height H was on average 1.2 m (cf. Table 1). Two outlet diameters D_o (25 and 50 mm) and three combinations of aeration sections were investigated: A, B and A+B (cf. Fig. 2

TABLE 1. Input parameters used for investigating the parametric sensitivity of the discharge model (B case, cf. Fig. 9). Geometry data for the A-case aeration are also given

Parameter	Default value	Changed values			
α (°)	19.0				
r_1 (m)	0.922				
r_3 (m) (B case)	0.215				
r_2 (m) (B case)	0.435	0.300	0.400	0.500	0.600
D_o (m)	0.025	0.020	0.023	0.027	0.030
H (m)	1.2	0.0	0.5	2.0	5.0
$\delta\epsilon$ (-)	0.0	−0.03	0.03	0.06	0.09
ϕ_w (°)	23.0	0.0	10.0	17.0	29.0
r_3 (m) (A case)	0.083				
r_2 (m) (A case)	0.215				

and Table 1). As expected, during all experiments mass flow occurred.

The following properties of the FCC powder used for the discharge experiments were determined: the internal friction angle δ, the wall friction angle ϕ_w for polished stainless steel, stainless steel sinterplate and aluminium, and the unconfined yield strength σ_y using a Jenike shear cell [14, 15]. As the porous stainless steel hopper wall is relatively smooth a value of 23° was taken for ϕ_w in the model calculations. Furthermore, the particle size distribution (psd), the minimum fluidisation velocity U_{mf}, the minimum bubbling velocity U_{mb}, the particle density and several bulk densities were determined. A summary of the results is given in Table 2.

The results of the particle discharge rate measurements are shown in Figs. 5 and 6. The aeration section used is registered with A, B and AB for A+B. With measurements 25/A, 25/B, 25/AB and 50/A, 50/AB the influence of orifice diameter and of the location of the aeration section was investigated. Measurements 50/A, 50/A/H< and 50/A/H≪ show the influence of the filling height of the bunker (cf. Fig. 6). First, some general phenomena, which appeared during the experiments, will be described. Next, the dependencies mentioned above will be discussed.

TABLE 2. Summary of FCC powder characterisation

Internal friction angle δ	30°
Unconfined yield strength σ_y	0 N
Wall friction angle ϕ_w polished SS	20°
20 μm sintered SS	30°
aluminium	18°
Minimum fluidisation velocity U_{mf}	1.54 mm s^{-1}
Minimum bubbling velocity U_{mb}	4.5 mm s^{-1}
Mean particle diameter d_p	64.5 μm
Weight fraction < 20 μm	0.15%
< 40 μm	10.0%
< 80 μm	79.2%
< 105 μm	96.6%
Particle density ρ_p	1477 kg m^{-3}
Bulk densities in Jenike shear cell	868 kg m^{-3}
loosely compacted	830 kg m^{-3}
compacted	900 kg m^{-3}
at U_{mf}	790 kg m^{-3}
at U_{mb}	617 kg m^{-3}
Mass absorption coefficient (^{137}Cs) α'	7.76×10^{-4} m^2 kg^{-1}

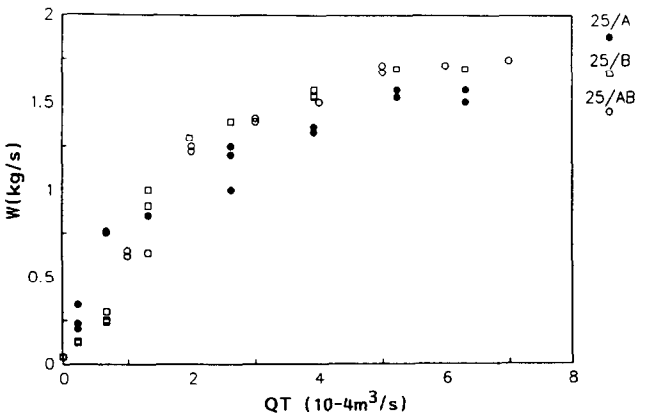

Fig. 5. Results of particle discharge rate measurements for 25 mm outlet diameter: 25/A, 25/B and 25/AB.

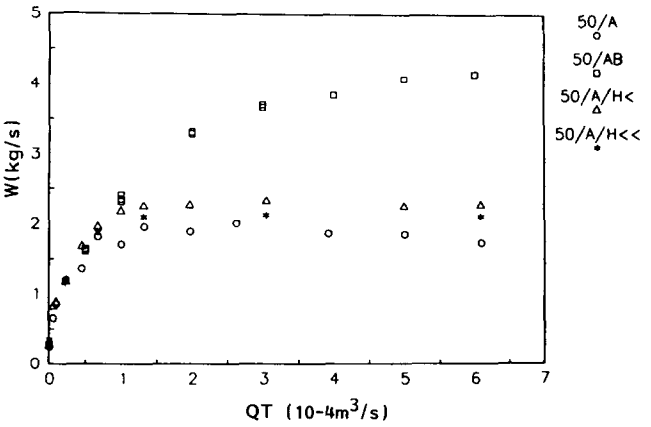

Fig. 6. Results of particle discharge rate measurements for 50 mm outlet diameter: 50/A, 50/AB, 50/A/H< and 50/A/H≪.

First of all, time is needed for the discharge flow to become constant with characteristic times that vary between 5 and 80 s for the different measurements. With a larger orifice and a lower aeration section these times are relatively short. Secondly, when the filling height in the hopper falls beneath a critical value, the discharge rate can suddenly increase to another constant. This is attributed to breakthrough of the aeration gas to the top of the bed, reducing the drag force. The critical filling height increases with increasing gas flow, as does the new discharge rate. Finally, the powder jet emerging from the bunker changes markedly in shape when the discharge rate increases, as has been observed before with fine powders [10]. At zero aeration, an underpressure is created and the jet contracts. When a small amount of gas is added, say 1×10^{-4} m^3 s^{-1}, a much thicker jet is seen. By adding more gas, this jet becomes fuller and starts to disperse.

Next, the various sets of measurements will be discussed. First, it can be seen in Figs. 5 and 6 that the addition of gas into the hopper increases the discharge rate, until a limiting gas flow is reached, after which this rate becomes constant. At high gas flow rates a minor decrease is seen in the 50/A case. Furthermore, when using aeration section B or AB, the maximum discharge flow is larger than when use is made of aeration section A. This is evident in case of the 50 mm orifice, but less evident for the 25 mm outlet, which

is due to the force exerted by upflowing gas on the particles above r_i, which becomes appreciable in case of the small aeration section A. The same amount of gas is added to a much smaller volume as in the case of B or AB, which is also the reason why the results of 25/B and 25/AB do not differ much. From this it is concluded, that the higher up the gas is added, the higher the maximum particle discharge rate becomes.

The influence of the orifice diameter depends on the amount of added gas. In case of zero aeration a factor of ~6–7 between the 50 and 25 mm orifice is measured. The Beverloo equation (1) predicts a dependency of $D_0^{2.5}$. Our experiments show an exponent of 2.7. When gas is added this exponent decreases, depending on the location of the aeration section.

The influence of the height is not very outspoken, cf. the curves 50/A, 50/A/H < and 50/A/H ≪. It is therefore concluded that the filling height indeed has a small influence on the particle discharge rate.

In situ bulk density measurements

During the discharge experiments the bulk densities at the outlet and at the bin/hopper junction were measured using gamma-ray absorption [3, 7, 8]. The mass absorption coefficient α' of the FCC powder was calibrated using a powder sample of known density and size (see Table 2).

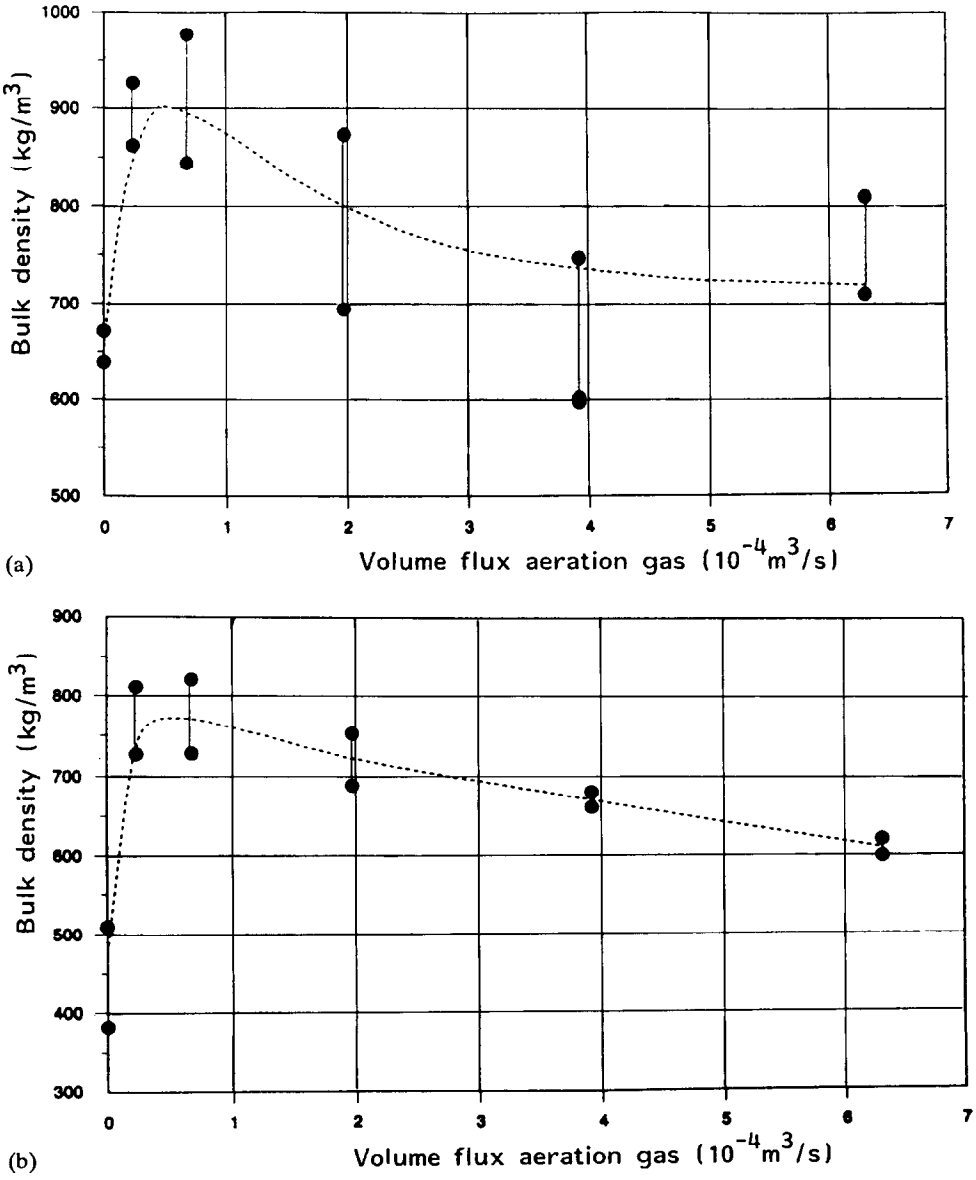

Fig. 7. *In situ* bulk density versus Q_T at the orifice for (a) the 25/A and (b) the 50/A case.

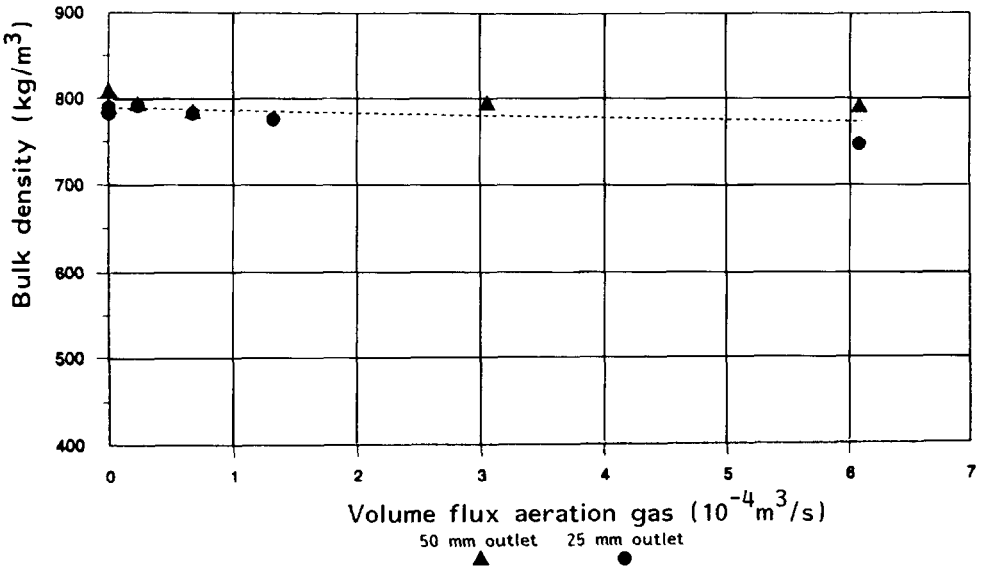

Fig. 8. *In situ* bulk density versus Q_T at the bin/hopper crossing for 25/A and 50/A.

The results of the bulk density measurements at the orifice are shown in Figs. 7(a) and (b) for the 25/A and 50/A cases, respectively. In measuring the bulk densities we took the changing absorption path length when increasing the aeration gas flow into account. In the case of the 50 mm orifice it was difficult to estimate the absorption path length for $Q_T = 0$, because the flow was sometimes pulsating. In that case a maximum path length was estimated, resulting in a calculated bulk density, which is a lower limit. The accuracy of the determined bulk densities is rather low due to the relatively short measuring times (24 to 100 s) and the small difference between the attenuated gamma-ray intensity I and the unattenuated intensity I_0: when the absorption length increases this error rapidly becomes smaller. Despite the relatively large errors ($\pm 10\%$ or ± 80 kg m^{-3}) two trends can be seen. In the case of gravity discharge an appreciable decrease in bulk density is measured at the orifice. This has been observed before [3, 7, 8]. Surprisingly, even at low aeration flows the density increases sharply again, levelling off to a value around ρ_{mf}. To our knowledge, this has not been observed before. For use in the model calculations the dashed curves were used. In Fig. 8 the results of the bulk density measurements at the bin/hopper junction are shown. In this case the data are much more accurate due to a much longer absorption path length and they show a constant bulk density during discharge, about equal to ρ_{mf} and independent of Q_T. Again, the dashed curve was used in the model calculations.

Evaluation of the improved model

The input parameters for the improved model described above which are related to the powder properties were taken from Table 2. For the filling height H of the powder in the bin a mean value was chosen, as the height changes during the batch experiments. Another necessary parameter for calculating the discharge rate is the radial solids stress at the bin/hopper junction. This value is a function of the filling height and was calculated with the condition of an active stress state in the bin using the theory of Walters [6]. As an aid for the interpretation of the experimental and theoretical results, the theoretical dependency of W on the input parameters was investigated. Some of these parameters will be discussed first. Thereafter, the comparison with experiment will be made.

The parameter sensitivity has been investigated as follows: W has been calculated for a chosen standard situation and in each following case a variable was changed. Of the 13 available parameters the five most important ones will be discussed below, namely: D_o, r_2, H, $\delta\epsilon$ and ψ_w. For each parameter four different values were chosen which together with the standard situation resulted in five curves in a W–Q_T diagram. The values used are tabulated in Table 1; the curves are shown in Figs. 9(a) to (e).

In general, the discharge with zero aeration is not affected by the height of the hopper r_1, the location of the aeration section (r_2 and r_3), the filling height H in the bin, the particle size d_p, the particle density ρ_p, and the radial stress at the bin/hopper junction. The influence of the particle size d_p and the particle density (or ϵ) can be explained by looking at the equation for the permeability eqn. (6). The discharge can be increased by increasing the orifice diameter D_o, showing indeed a proportionality to $\rho_b D_o^{2.5}$ as in the Beverloo equation (cf. eqn. (1) and Fig. 9(a)). Increasing the hopper angle θ_w (and thus increasing the bin diameter) or the wall

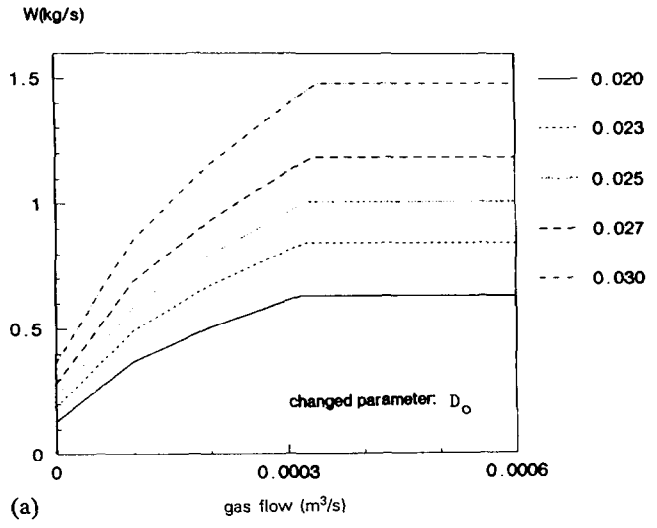

(a)

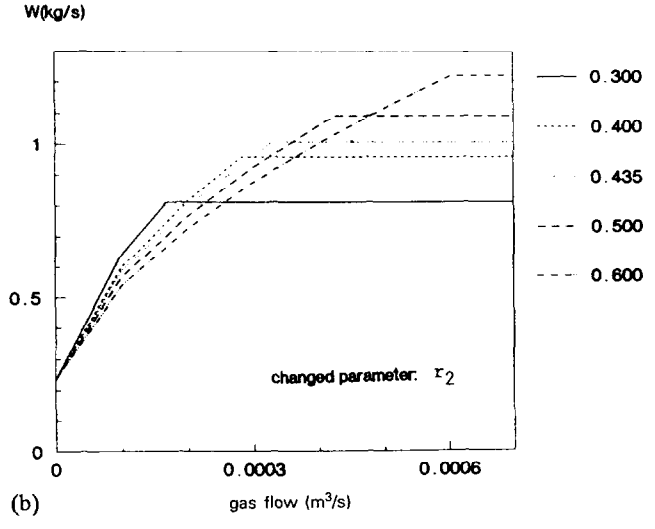

(b)

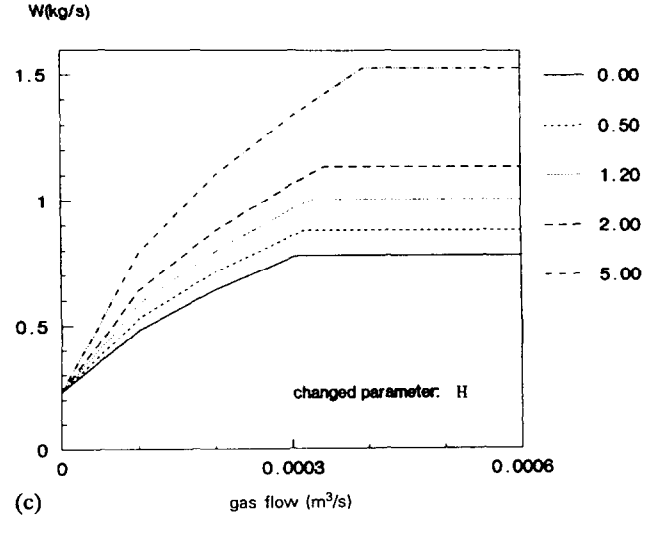

(c)

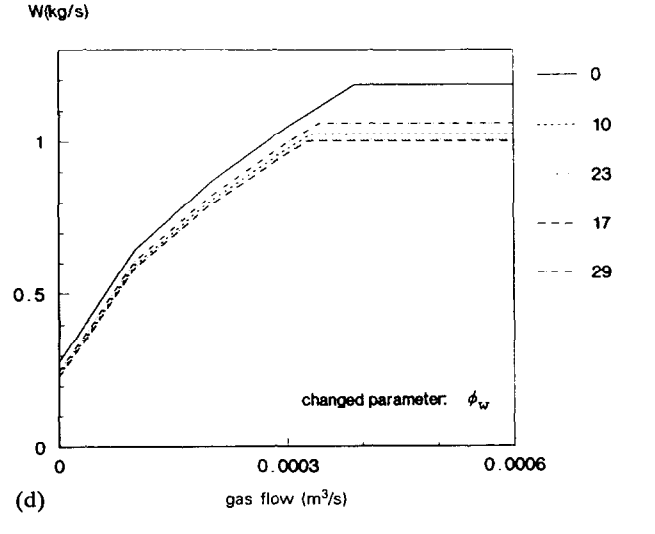

(d)

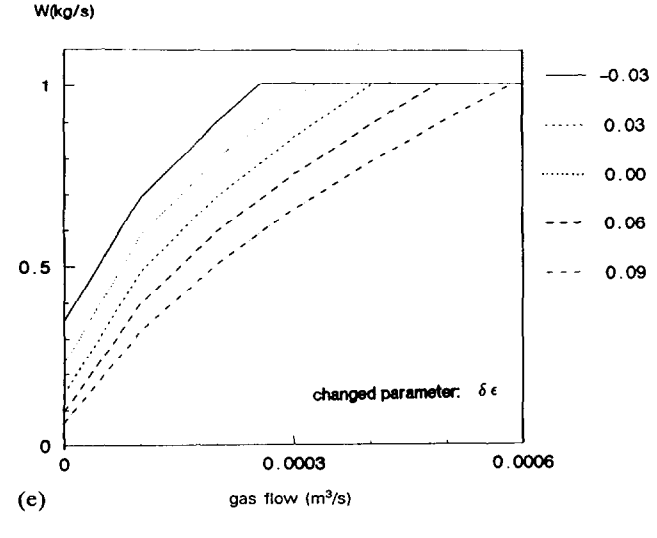

(e)

Fig. 9. Parametric sensitivity of the model predictions: (a) outlet diameter D_o; (b) end aeration section r_2; (c) height of bin H; (d) wall friction angle ϕ_w; (e) total dilation in hopper $\delta\epsilon$.

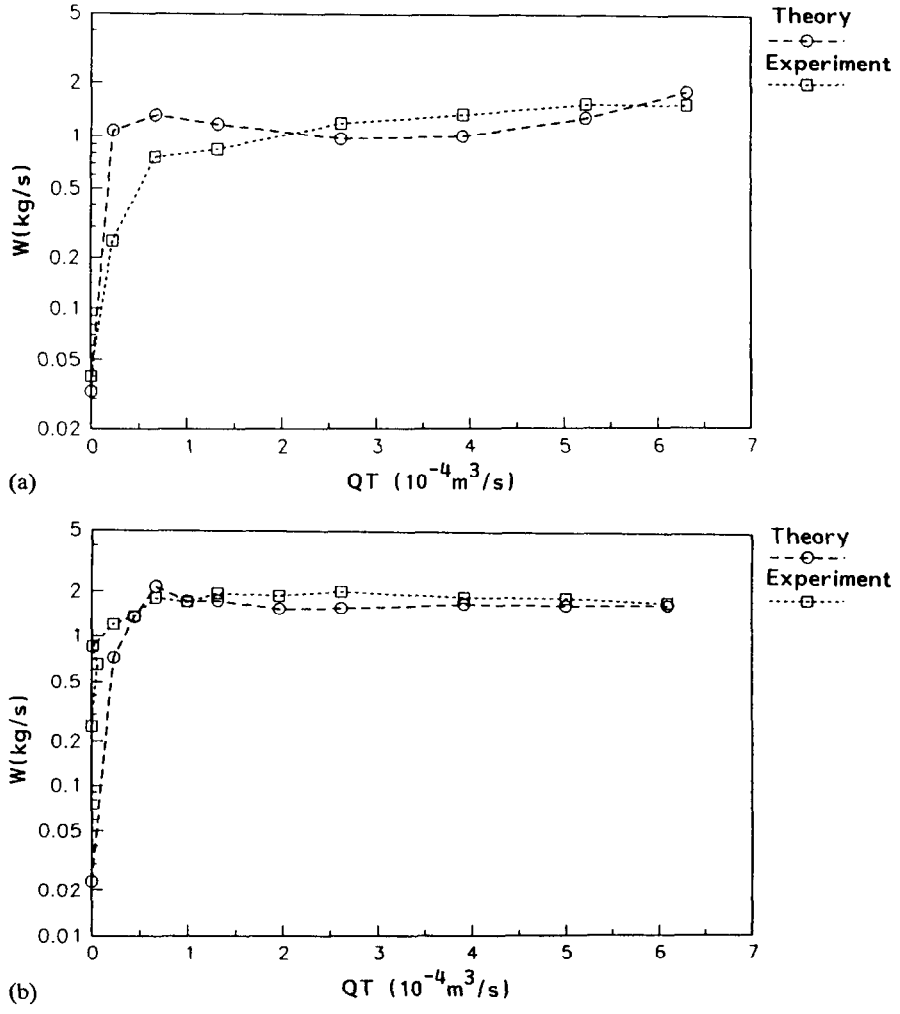

Fig. 10. Comparison theory and experiment with *in situ* measured bulk densities for 25/A (a) and 50/A (b).

friction angle ϕ_w leads to a decrease in discharge. Furthermore, an increase in $\delta\epsilon$ also decreases the discharge rate due to the negative pressure gradient created at the outlet. Because this pressure gradient is influenced by the location of the aeration section, this changes the influence of $\delta\epsilon$, e.g. a lower aeration section leads to a larger gradient and thus to a lower discharge rate for the same $\delta\epsilon$. This is of course not in accordance with reality, because for $Q_T=0$ the position of the aeration section should not be relevant.

The next part of the aerated discharge curve, *i.e.* $Q_T\neq 0$, is affected by all parameters, except the radial stress at r_1. This parameter does not show any influence until very large values are chosen. Naturally, an increase in orifice diameter enlarges the mass flow, but Beverloo (eqn. (1)) is not valid anymore as the pressure difference Δp_0 is added to the equation of motion and this term is a function of d_p and ρ_b. With respect to the aeration section it can be said that enlarging this section can lead to a decrease as well as an increase in discharge. Enlarging by lowering the lower boundary r_3 leads to an increase and enlarging by increasing the upper boundary r_2 decreases the discharge (cf. Fig. 9(b)). This is caused by the fact that the conditions near the orifice are important and thus more injection of gas near the orifice will increase the flow. The maximum discharge is also influenced by r_2, as observed both in the experiments (see above) and in, e.g., Fig. 9(b). Unexpectedly, the aerated discharge can be increased by increasing the filling height H in the bin (cf. Fig. 9(c)). This can be explained by the fact that more powder in the bin will increase the fraction of the added gas going downwards, and thus increase the positive pressure gradient and the discharge rate. In the experiment the sensitivity is indeed much larger than expected from a friction-dominated flow regime. An increase in friction angles diminishes the flow, as expected (cf. Fig. 9(d)). Finally, a larger $\delta\epsilon$ decreases the discharge rate, because the effective gas flow is reduced, see eqn. (30) and Fig. 9(e).

For comparison of model predictions with experimental results two different W–Q_T diagrams have been

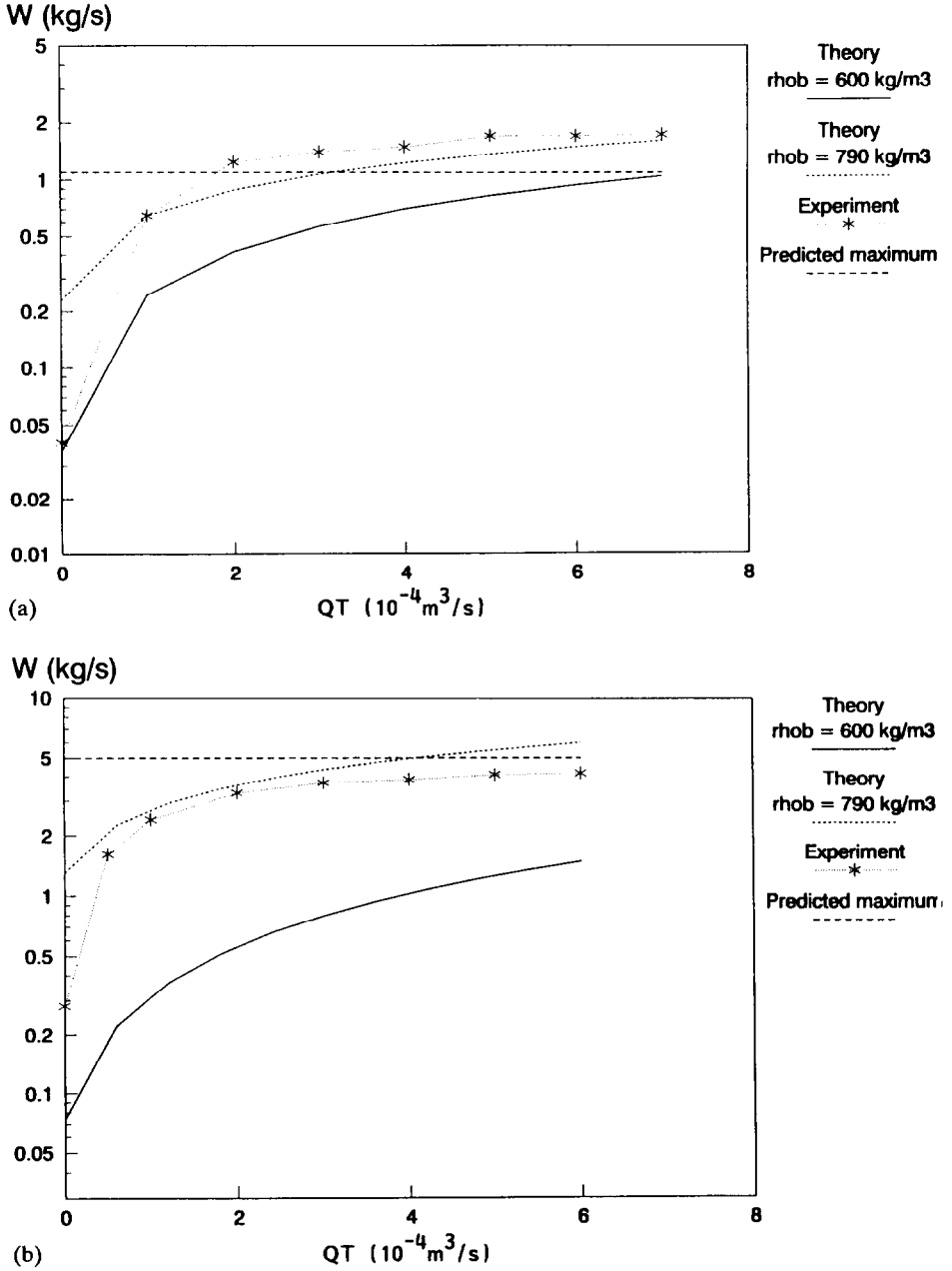

Fig. 11. Comparison theory and experiment using a constant bulk densities through the hopper for 25/AB (a) and 50/AB (b).

plotted. The first type uses the *measured* bulk densities at the outlet and the bin/hopper junction. This has been done for measurements 25/A and 50/A in Figs. 10(a) and (b). For the other cases the necessary bulk densities at the orifice are unknown, and therefore a second way of comparison is chosen. Two model curves were calculated for different outlet bulk densities to compare with the experimental curve. This has been done for measurements 25/AB and 50/AB in Figs. 11(a) and (b). For all curves, the predicted maximum discharge rate is also shown and it should be noted that this maximum is independent of the dilation $\delta\epsilon$.

For measurement 25/A the deviation with prediction varies from -25% at $Q_T=0$, via $+400\%$ at $Q_T=0.23\times10^{-4}$ m^3 s^{-1}, to $\pm20\%$ for large gas flows (cf. Fig. 10(a)). The uncertainty in the measured bulk density is about 50–100 kg m^{-3} (see Fig. 7(a)). This influences the deviations significantly, because the theoretical predictions are very sensitive to the bulk density at the outlet (cf. Fig. 9(e)). Thus, the determination of these densities has to be very accurate. For the 50/A case the curves almost overlap, except for $Q_T=0$ (see Fig. 10(b)). The relative errors run from -90% for $Q_T=0$ to less than 5% for large gas flows. The cause of the large deviation for small gas flows is the

steepness of the curve for the local density at the outlet at low gas flows. Here, too, precise bulk densities are needed, but it is clear that the introduction of the dilation improves the predictions of the model dramatically.

In Fig. 11 the model curves drawn have a constant dilation or outlet density for the whole aeration range. For these densities the values of ρ_{mf} and ρ_{mb} (see Table 2) were chosen as an upper and lower limit, respectively. The comparisons show that for the 25/AB and 50/AB cases the bulk density as a function of the gas flow must behave similarly to 25/A and 50/A. An outlet density of around 600 kg m^{-3} at $Q_T = 0$, which rapidly increases with Q_T to 790 kg m^{-3}, strongly improves the model predictions.

The question now arises as to how to predict these bulk densities. It does not seem possible to relate the local densities to the solid stresses, because this would predict a very small dilation independent of the gas flow, and because at the bin/hopper junction the solids stress is positive, but the bulk density roughly equals ρ_{mf}, matching a zero stress. From the results of the density measurements at the bin/hopper junction it seems that the powder could be fluidised during flow. This would implement a stress equal to zero everywhere in the bunker. Considering the equation of motion, this means that the terms σ_r/r and $d\sigma_r/dr$ are zero and an equation analogous to Bernouilli's equation is obtained. This has been the basis for the 'kinetic' approaches (cf. refs. [10] and [13]). One could imagine that for zero aeration the powder will dilate as much as possible, *i.e.* up to the minimum bubbling point, where the so-called continuity wave velocity (e.g. derived from the Richardson–Zaki relationship) overhauls the elastic wave velocity, as has been derived by, for example, Foscolo and Gibilaro [16]. When aeration gas is added the density quickly increases to ρ_{mf}, maximizing the discharge rate and minimizing its potential energy. Then, indeed as observed, the bulk density varies with gas velocity, and a minimum density can be calculated from the maximum expansion at fluidisation, *i.e.* the minimum bubbling point. For the FCC powder this indeed yields a value of around 600 kg m^{-3} (see Table 2).

Conclusions

The introduction of gas through a porous cone section strongly increases the discharge rate of FCC powder by up to a factor of 40 for the 25 mm orifice.

Lowering the aeration section increases the particle discharge rate for small gas flows, but reduces the discharge rate for large gas flows.

When the bunker is aerated the filling height has a larger influence on the particle discharge rate than is expected from friction-dominated (e.g. Mohr–Coulomb type) flow, because of breakthrough of aeration gas to the top of the bed.

The bulk density at the bin/hopper junction is the same for all flow conditions and equals the bulk density at minimum fluidisation ρ_{mf}. However, the bulk density at the outlet is a function of the amount of added gas. With increasing gas flow, this density at the outlet reaches a maximum roughly equal to ρ_{mf}. The largest expansion observed coincides with the maximum bed expansion in a fluidisation test.

For zero aeration gas a large dilation (15–35%) was observed. With these data the model predictions improved from 600% overestimation error to 25–90% underestimation for pure gravity discharge, and from 100% to 0–20% error for aerated discharge. The introduction of the dilation strongly improves the model predictions: a much lower mass flow in case of zero aeration and a maximum for high gas flows. A shortcoming of the model is then that the location of the aeration section influences the discharge rate for $Q_T = 0$. In reality this aeration section is not used at all, and thus should not have any influence.

The model needs the bulk density at the outlet in order to have a predictive value. This dilation cannot be predicted from the powder compressibility, but seems to be linked to the maximum dilation measured in a fluidisation test. More accurate in-situ bulk density measurements for different materials are necessary to confirm this approach.

List of symbols

A	area, m^2
A	constant defined in eqn. (17), Pa m^4
A_a	parameter defined in eqn. (11), Pa m^{-1}
$A_{a,\,max}$	parameter defined in eqn. (24), Pa m^{-1}
B_i	constant defined in eqn. (17), Pa m
C_i	constant defined in eqn. (17), Pa m^{-1}
D	constant defined in eqn. (18), –
D_a	constant defined in eqn. (3), –
D_o	hopper outlet diameter, m
d_p	mean particle diameter, m
E	constant defined in eqn. (3), –
F	constant defined in eqn. (3), –
g	gravitational acceleration, m s^{-2}
H	filling height in bin, m
I	attenuated radiation rate, s^{-1}
I_0	unattenuated radiation rate, s^{-1}
K	ratio between principal stresses, –
K_p	coefficient of permeability, m^2 s kg^{-1}
k	constant in eqn. (1), –
p	fluid pressure, Pa
Q	effective gas flow, m^3 s^{-1}

Q_T total gas flow, $m^3\ s^{-1}$
r radial coordinate, m
r_0 radial distance of apex to outlet, m
r_1 radial distance of apex to hopper end, m
r_2 radial distance apex to upper boundary aeration section, m
r_3 radial distance apex to lower boundary aeration section, m
r_i radial distance apex to lower position at which dp/dr is zero, m
r_m radial distance at which the stress has a minimum, m
U_α inlet gas velocity defined by eqn. (5), $m\ s^{-1}$
U_{mf} minimum fluidisation gas velocity, $m\ s^{-1}$
U_{mb} minimum bubbling gas velocity, $m\ s^{-1}$
u relative gas velocity, $m\ s^{-1}$
V solids volume flow defined in eqn. (3), $m^3\ s^{-1}$
v particle velocity, $m\ s^{-1}$
W particle discharge rate, $kg\ s^{-1}$
x r/r_0, –
y r_1/r_0, –
z_2 r_2/r_0, –
z_3 r_3/r_0, –
z_m r_m/r_0, –

Greek letters

α half hopper angle, –
α' mass absorption coefficient, $m^2\ kg^{-1}$
δ internal friction angle, –
Δp_0 pressure difference over orifice, Pa
ϵ bed voidage, –
θ angular coordinate, –
μ dynamic viscosity, Pa s
ρ_b bulk solids density, $kg\ m^{-3}$
ρ_p particle density, $kg\ m^{-3}$
ρ_{mf} bulk solids density at minimum fluidisation, $kg\ m^{-3}$
σ_y unconfined yield stress, Pa
σ_r solids stress in r-direction, Pa
σ_θ solids stress in θ-direction, Pa
σ_ψ solids stress in ψ-direction, Pa
θ angular coordinate, –
τ shear stress, Pa
ϕ_w wall friction angle, –
ψ azimuthal coordinate, –

References

1 N. P. Cheremisinoff (ed.), *Encyclopedia of Fluid Mechanics,* Vol. 4, Gulf, Houston, USA, 1986, pp. 145–194.
2 B. J. Crewdson, A. L. Ormond and R. M. Nedderman, *Powder Technol., 16* (1977) 197.
3 C. D. Spink and R. M. Nedderman, *Powder Technol., 21* (1978) 245.
4 R. M. Nedderman, U. Tuzun and R. B. Thorpe, *Powder Technol., 35* (1983) 69.
5 D. M. Walker, *Chem. Eng. Sci., 21* (1966) 975.
6 J. K. Walters, *Chem. Eng. Sci., 28* (1973) 13 and 28 (1973) 779.
7 D. J. van Zuilichem, N. D. van Egmond and J. G. de Swart, *Powder Technol., 10* (1974) 161.
8 K. E. Fickie, R. Mehrabi and R. Jackson, *AIChE J., 5* (1989) 853.
9 J. Ravi Prakash and K. Kesava Rao, *Chem. Eng. Sci., 43* (1988) 479.
10 C. S. Papazoglou and D. L. Pyle, Powder Technol., 71 (1970) 9.
11 H. K. Altiner, *Ph.D. Thesis,* univ. of Cambridge, UK, 1975.
12 H. K. Altiner, *AIChE Symp. Ser., 222* (1983) 55.
13 W. Resnick, Y. Heled, A. Klein and E. Palm, *Ind. Eng. Chem. Fundam., 5* (1966) 392.
14 A. W. Jenike, *Utah Univ., Bull., 123* (1964).
15 L. Svarovsky, *Powder Testing Guide: Methods of Measuring the Physical Properties of Bulk Powders,* Elsevier, Barking, 1987.
16 P. U. Foscolo and L. G. Gibilaro, *Chem. Eng. Sci., 39* (1983) 1667.